THE ASTROPHYSICAL JOURNAL, 282:574–583, 1984 July 15

CONVECTION IN THE ENVELOPES OF RED GIANTS

H. M. ANTIA, S. M. CHITRE, AND D. NARASIMHA
Tata Institute of Fundamental Research
Received 1983 November 4; accepted 1984 January 31

ABSTRACT

The nature of convection in the envelopes of red giants is investigated, and the linear convective modes are computed to demonstrate the consistency of the mixing length theory. The mixing length at a given depth is tentatively identified with an equivalent width of the luminosity profile of the convective eigenmodes. The dominant convective element turns out to be comparable in size to the radius of the star, and this could account for the observed irregular variations in red giants.

Subject headings: convection — stars: interiors — stars: late-type

I. INTRODUCTION

A majority of well observed red giants and supergiants appear in the classical list of variable stars (Strohmeier 1972). These variables can be divided into two groups (Payne-Gaposchkin 1954) depending on the amplitude A of variation, in the visual magnitude: the long period (Mira) variables ($A > 2.5$ mag) and the red semiregular and irregular variables ($A < 2.5$ mag). Even for the most regular Mira variables the successive light curves are never identical, but exhibit irregularity both in period and in amplitude.

The main distinctive characteristic of the red semiregular and irregular variables is their small amplitude which rarely exceeds 2 mag in the visible. The light variations in these stars are cyclic or irregular rather than periodic. In most of these stars there is not even an approximately constant interval between successive maxima (or minima) and often there are long periods of completely irregular behavior. There are times when the star may remain at virtually constant brightness. In some of these stars detailed investigations have shown that the light curves may be explained as a result of the interference of two or more periodic oscillations, each of which may be more or less regular and varying independently (Wood 1975).

Fox and Wood (1982) have made an exhaustive study of linear, nonadiabatic pulsation of long-period variables. The growth rates obtained from these calculations show that in a star of given mass, the fundamental mode is strongly driven at high luminosities, whereas the first overtone tends to have the higher growth rates at lower luminosities. This is consistent with the results obtained from nonlinear pulsation calculations (Keeley 1970; Wood 1974; Tuchman, Sack, and Barkat 1979) which show that a star switches to lower order pulsation modes as it evolves up the giant branch. For the Mira variables the pulsation theory seems to provide a plausible explanation though the mode of pulsation is still a matter of dispute (Willson 1982; Wood 1982). Even some of the nonregular variables may also be pulsating (Stothers 1972); in fact, in at least one case (α Orionis or Betelgeuse) the changes in angular diameter are claimed to have been actually measured by Pease in 1926.

A novel mechanism for producing irregular and semiregular variability in red giants has been suggested by Schwarzschild (1975). In his model the luminosity variations are caused by surface temperature fluctuations in giant supergranules produced by the extensive convection zones in red giant stars. He has put forth some qualitative arguments to support his hypothesis that in these stars the dominant convective elements will have a very large size comparable to the stellar radius. It is further argued that this scenario can also explain the observation of linear polarization of the visual light of red giants and supergiants. One of the aims of the present work is to test Schwarzschild's hypothesis regarding the length-scale of the dominant convective element by studying the linear stability of convective modes.

The stability of linear convective modes in the solar envelope model has been studied by Antia, Chitre, and Narasimha (1983, hereinafter referred to as Paper I) to find that the inclusion of turbulent pressure yields two distinct peaks in the plot of growth rate versus wavelength for these modes. This provides a very natural explanation for the occurrence of two distinct length scales of solar convection corresponding to granulation and supergranulation. Further, for a reasonable choice of parameters it is possible to get these scales in reasonable accord with observations. It is therefore of interest to study the linear stability of convective modes in red giants to find out the dominant scale of convective elements.

The question of the stability of convective modes in a red giant was addressed by Hart (1973) from a completely different point of view, namely, for examining the consistency of the mixing length theory. He studied the convective modes in the adiabatic approximation to find that the convective flux due to each of the individual modes has a maximum near the base of the convection zone. It then becomes impossible to construct a linear superposition of these modes which can reproduce the convective flux profile in these models. A similar conclusion was reached by Hart for the solar case too. However, Narasimha and Antia (1982, hereinafter referred to as Paper II) have demonstrated that once the effects of turbulence are included in the calculations of linear convective modes, it is possible to construct a linear superposition of these modes which can reproduce the convective flux throughout the solar convection zone. In the present study we wish

to extend this work to the envelopes of red giants which have a substantially different structure. Finally, we explore the possibility of identifying the mixing length with some characteristic scale associated with the convective eigenmodes.

II. EQUILIBRIUM STELLAR MODEL

The envelopes of red giants are characterized by extensive convection zones with significant superadiabatic gradients. In such a situation the turbulent pressure is expected to be very important in determining the equilibrium model. It turns out that the stellar models computed with the local mixing length formulation yield unrealistically large gradients of turbulent pressure in certain regions of the convection zone (Baker and Gough 1979; Antia, Chitre, and Narasimha 1983). In order to circumvent this difficulty we replace the standard expression for convective velocity by a differential equation similar to the one used by Shaviv and Chitre (1968). By introducing nonlocality in this manner the velocity profile is smoothed out, and this reduces the gradient of turbulent pressure. We describe below the prescription used to calculate the convective velocity and the convective flux.

With the notation of Paper I, convective flux is given by the usual expression of the mixing length theory,

$$F^C = \alpha\rho C_p W L \frac{T}{H_p}(\nabla - \nabla') = -\alpha\rho W L \frac{\Gamma}{\Gamma + 1}\frac{ds}{dr}, \tag{1}$$

where Γ is the efficiency of convection given by (cf. Henyey, Vardya, and Bodenheimer 1965)

$$\Gamma = \frac{\rho C_p W}{8\sigma T^3}\left(\frac{1 + y(L\kappa\rho)^2}{L\kappa\rho}\right). \tag{2}$$

Here the factor inside the parenthesis is introduced to yield the correct value in the optically thick as well as the optically thin limit, and y is a parameter of order unity. We calculate the mean convective velocity by including the aerodynamic drag experienced by moving elements, essentially following the treatment of Shaviv and Chitre (1968). A distinguishing feature of this scheme is the asymmetry between rising and falling convective elements. A descending element is expected to be distorted because of the eddies generated around it during its motion through a system of ascending elements. The resistance that the element suffers will manifest itself as a drag which is mainly determined by the energy dissipation of the eddies in the wake. When this drag is taken into account, the governing equation of motion becomes

$$\frac{dW^2}{dr} = \frac{\beta g Q L}{H_p}(\nabla - \nabla_{ad}') - \frac{DW^2}{L}, \tag{3}$$

where β is a parameter of order unity and $D = 4C_D$, where C_D is the aerodynamical drag coefficient, which is of order unity.

Adopting these equations along with the usual equilibrium equations (cf. Henyey, Vardya, and Bodenheimer 1965), we can calculate the envelope model for a red giant. In the atmosphere ($\tau < \frac{2}{3}$) we use the following (T-τ) relation due to Krishna-Swamy (1966):

$$T^4 = 0.75 T_e^4(\tau + 1.4 - 0.82e^{-2.54\tau} - 0.25e^{-30\tau}). \tag{4}$$

For numerical solution of these equations we use the Hamming's fourth order predictor-corrector method (cf. Ralston 1965). The integration is started from some point inside the convection zone and is carried out both upward and downward. The starting values of T, ρ, M_r, and W are adjusted to satisfy the following conditions:

1. $T = T(\tau = \frac{2}{3})$ at $r = R$,
2. $\rho \to 0$ as $\tau \to 0$,
3. $M_r \to M$ as $\rho \to 0$,
4. $W = 0$ at the base of the convection zone.

In the above, R is the stellar radius and M the stellar mass.

We consider the same parameters as those discussed by Schwarzschild (1975): $M = 0.65\ M_\odot$, $L = 8000\ L_\odot$, $T_e = 3600$ K, $X = 0.7$, $Y = 0.299$, $Z = 0.001$. Further, we choose the mixing length parameters, $\alpha = \frac{1}{2}$, $\beta = \frac{1}{8}$, $y = \frac{1}{2}$, $D = 1$, $c = 1$, and compute the stellar envelope models for different values of the ratio of mixing length to pressure scale height. Table 1

TABLE 1

PROPERTIES OF ENVELOPE MODELS FOR THE RED GIANT CORRESPONDING TO VARIOUS VALUES OF L/H_p AND c

Mixing Length Formalism	c	L/H_p	Depth of Convection Zone (km)	Radial Distance of the Base of Convection Zone	Maximum Value in Convection Zone					e-Folding Time of C1-Mode ($l = 1$) (days)
					$(\nabla - \nabla_{ad}')$	W (km s^{-1})	x	Mach No.	y	
A, nonlocal	1	2	1.59×10^8	0.005 R	4.37	8.28	0.46	0.71	1.05	1.6
B, nonlocal	1	1	1.40×10^8	0.13 R	5.41	7.17	0.45	0.70	1.24	31.0
C, nonlocal	1	0.75	1.27×10^8	0.20 R	7.23	5.02	0.36	0.58	1.59	38.5
D, nonlocal	0	1	1.42×10^8	0.11 R	5.04	6.87	0.00	0.58	0.00	29.0
E, local	1	1	1.32×10^8	0.17 R	11.65	8.90	0.30	0.57	12.03	69.3
F, local	0	1	1.36×10^8	0.15 R	5.54	8.63	0.00	0.57	0.00	37.5

summarizes some of the characteristics of these models, where we have also included models without turbulent pressure ($c = 0$) as well as those calculated by using the local mixing length theory. It can be seen that the models depend rather sensitively on the mixing length. For $L = 2H_p$ the convection zone extends over 99.5% of the stellar radius, while for $L = H_p$ it shrinks to only 87% of the stellar radius. All the models are characterized by highly superadiabatic region near the top of convection zone where the value of $(\nabla - \nabla_{ad}')$ is much greater than unity. Further the degree of superadiabaticity in the region increases as L/H_p is decreased; on the other hand, the convective velocity which attains the maximum value somewhere in the middle of convection zone increases with increasing L/H_p. In order to demonstrate the importance of turbulent pressure, we have shown the maximum value in the convection zone of $x = P_t/(P_t + P)$ and $y = |\nabla P_t/(\nabla P_t + \nabla P)|$ in Table 1. It can be seen that in all the models (with $c \neq 0$) the turbulent pressure becomes comparable to the gas pressure in the highly superadiabatic region near the top of convection zone where the Mach number of convective motion is typically 0.5–0.75. Further, in all the models the turbulent pressure gradient exceeds the total pressure gradient in some region of the convection zone. In the models using the nonlocal version of mixing length theory this happens in regions where the turbulent pressure decreases inwards owing to a strong density inversion.

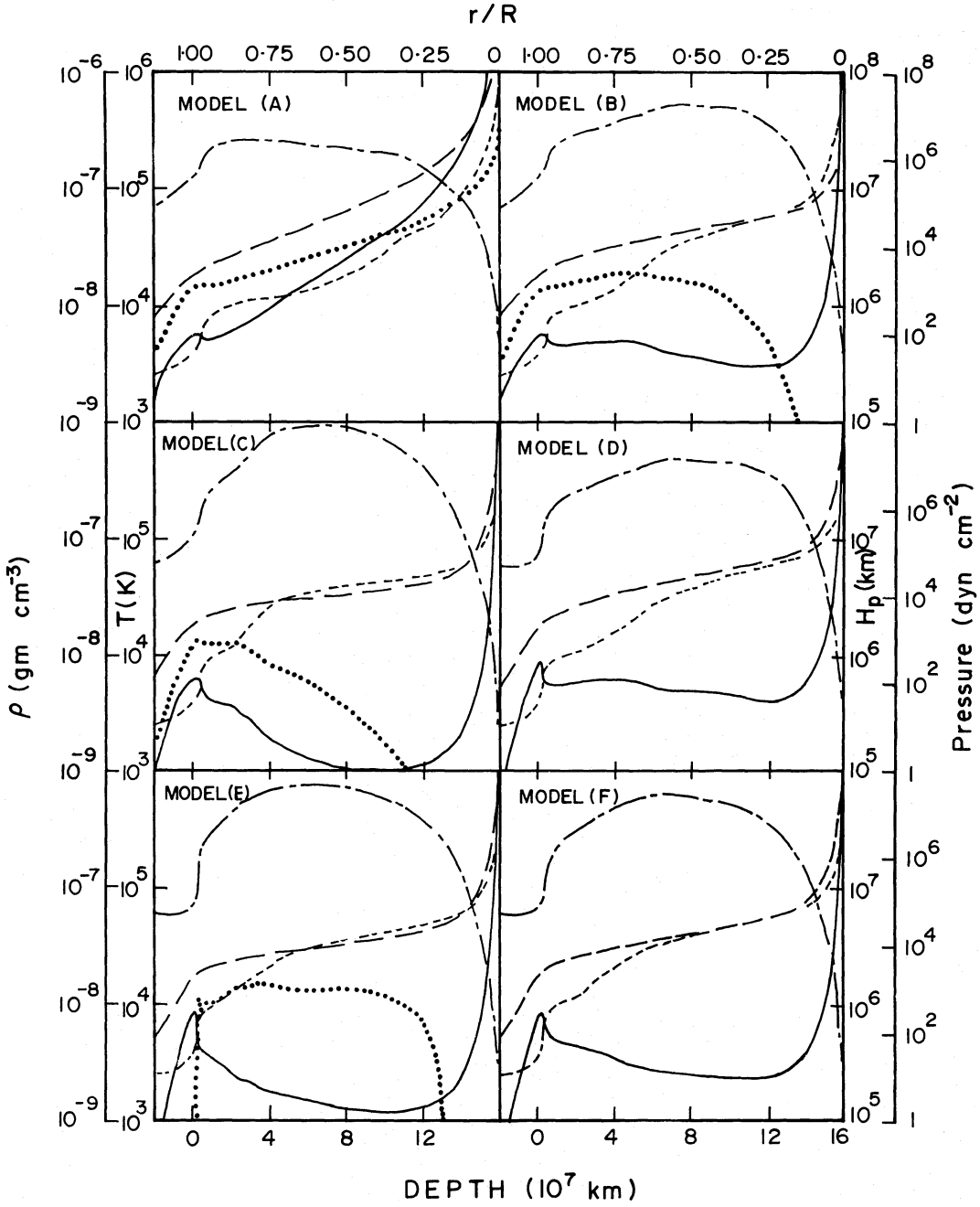

FIG. 1.—The run of physical variables, ρ (*continuous curve*), T (*short dashed curve*), total pressure (*long dashed curve*), H_p (*dot-dashed curve*), and turbulent pressure (*dotted curve*) as functions of depth is displayed for models A–F.

However, in model E, which uses the local mixing length theory, the turbulent pressure gradient becomes some 12 times the total pressure gradient and the gas pressure starts decreasing inward. Such a situation is clearly very unrealistic, and it also causes serious numerical problems because of which it is extremely difficult to compute models incorporating turbulent pressure in the local mixing length formulation. This prompted us to resort to some approximate description which incorporates nonlocality in the formalism.

The profiles of temperature, density, total pressure, turbulent pressure, and total pressure scale height H_p as a function of depth are displayed in Figure 1 for the six models listed in Table 1. All the models show significant density inversion in some regions, and the extent of density inversion decreases as L/H_p is increased. For example, for model A with $L = 2H_p$ the region of density inversion is rather narrow even though the turbulent pressure is included. Just as in the solar case (cf. Paper I), here also we find that the inclusion of turbulent pressure results in a substantial decrease in the density gradient, resulting in extensive regions with density inversion. Figure 2 displays the profile of convective velocity, superadiabatic gradient, and the critical growth rate

$$\omega_{cr} = g\left[-\frac{T}{P}\left(\frac{\partial\rho}{\partial T}\right)_P(\nabla - \nabla_{ad}')\right]^{1/2}, \tag{5}$$

in models A and B. It can be seen that the superadiabatic gradient shows three peaks corresponding to the three ionization zones (H^+, He^+, He^{++}), and further its value is significant almost throughout the convection zone. While ω_{cr} also shows the three peaks corresponding to the ionization regions, in addition it has a very broad peak near the base of the convection zone. In outer layers ω_{cr} is essentially determined by $(\nabla - \nabla_{ad}')$, and hence it shows the three peaks in the regions where ∇_{ad}' is reduced because of ionization. The first of these peaks is particularly prominent because of a substantial reduction in ∇_{ad}' due to the high turbulent pressure gradient in that region. Near the base of the convection zone ω_{cr} is significantly affected by the variation in g which increases almost as $1/r^2$. This leads to a rather broad peak near the base of the convection zone. This peak is even more prominent in models where the convection zone extends further down; particularly for model A, which has the convection zone extending up to $r \approx 0.005\ R$, the peak is abnormally high.

It is interesting to note that the pressure scale height in the solar convection zone varies from 150 km at the top to

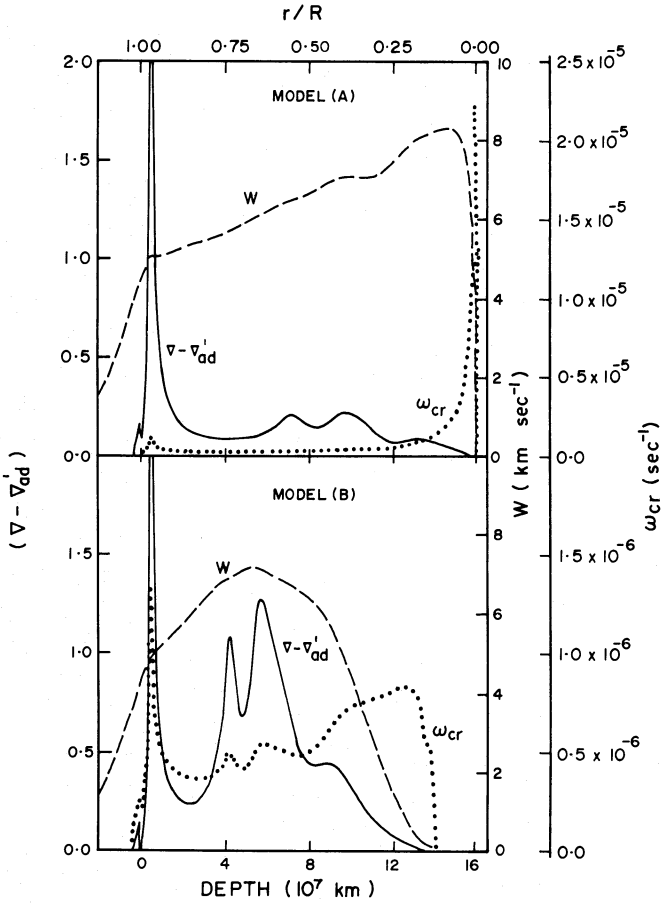

FIG. 2.—The superadiabatic gradient $(\nabla - \nabla_{ad}')$ (*continuous curve*), mean convective velocity W (*dashed curve*), and critical growth rate ω_{cr} (*dotted curve*) are shown as functions of depth for models A and B.

about 60,000 km at the bottom, a variation by a factor of 400. This contrasts with the red giant where the scale height variation is less than by a factor of 10. We therefore expect only a few convective modes to be excited in the case of the red giant.

III. LINEAR STABILITY ANALYSIS

We have adopted the usual equations of fluid dynamics as applicable to a viscous thermally conducting fluid, incorporating the turbulent pressure. Except for equations (1)–(3) of § II describing convective flux and convective velocity, the rest of the equations are identical to the ones described in Paper I. We follow the usual procedure to linearize these equations, and, using the notation of Paper I, the linearized equations can be written as follows:

$$\frac{dv_r}{dr} = -\left(\frac{2}{r} + \frac{1}{\rho_0}\frac{d\rho_0}{dr}\right)v_r + \frac{l(l+1)}{r}v_h - \frac{\omega}{\rho_0}\rho_1 , \tag{6}$$

$$\frac{4\mu_{t0}}{r}\frac{dv_r}{dr} - \frac{d\mathscr{P}_r}{dr} - \frac{dP_{t1}}{dr} = \left(\omega\rho_0 + \frac{4\mu_{t0}}{r^2}\right)v_r - \frac{2\mu_{t0}}{r^2}l(l+1)v_h - \frac{l(l+1)}{r}\mathscr{P}_h + g\rho_1 , \tag{7}$$

$$\mu_{t0}\frac{dv_h}{dr} = -\frac{\mu_{t0}}{r}v_r + \frac{\mu_{t0}}{r}v_h - \mathscr{P}_h , \tag{8}$$

$$\frac{2\mu_{t0}}{r}\frac{dv_r}{dr} + \frac{d\mathscr{P}_h}{dr} = \frac{2\mu_{t0}}{r^2}v_r - \left(\omega\rho_0 + \frac{2l(l+1)}{r^2}\mu_{t0} - \frac{2\mu_{t0}}{r^2}\right)v_h - \frac{1}{r}\mathscr{P}_r - \frac{3}{r}\mathscr{P}_h - \frac{P_{t1}}{r} , \tag{9}$$

$$\frac{\Gamma_0}{\Gamma_0+1}\frac{K_{t0}T_0}{C_{p0}}\frac{ds_1}{dr} = -F_r^C + \frac{F_0^C}{\Gamma_0+1}\left[\left(2+\frac{1}{2}\Gamma_0\right)\frac{\rho_1}{\rho_0} - (2-\Gamma_0)\frac{T_1}{T_0} + \frac{\kappa_1}{\kappa_0} + \frac{C_{p1}}{C_{p0}}\right] + \frac{(1+1/2\Gamma_0)}{(1+\Gamma_0)}\frac{F_0^C}{P_{t0}}P_{t1} , \tag{10}$$

$$\frac{4}{3\kappa_0\rho_0}\frac{dJ_1}{dr} = -F_0^R\left(\frac{\kappa_1}{\kappa_0} + \frac{\rho_1}{\rho_0}\right) - F_r^R , \tag{11}$$

$$\frac{dF_r^R}{dr} = -4\kappa_0\rho_0\left[(J_0 - \sigma T_0^4)\left(\frac{\kappa_1}{\kappa_0} + \frac{\rho_1}{\rho_0}\right) - 4\sigma T_0^3 T_1\right] - \left(4\kappa_0\rho_0 + \frac{l(l+1)}{r^2}\frac{4}{3\kappa_0\rho_0}\right)J_1 - \frac{2}{r}F_r^R , \tag{12}$$

$$P_{t0}\frac{dv_r}{dr} + \frac{dF_r^R}{dr} + \frac{dF_r^C}{dr} = -\left[\frac{2}{r}P_{t0} + \rho_0\frac{dE_{t0}}{dr} - \frac{\rho_0 T_0 C_{p0}}{H_p}(\nabla - \nabla_{ad}')\right]v_r + \frac{P_{t0}}{r}l(l+1)v_h + \frac{3}{2}\omega\frac{P_{t0}}{\rho_0}\rho_1$$
$$- \left[\omega\rho_0 T_0 + \frac{l(l+1)\Gamma_0}{r^2(\Gamma_0+1)}\frac{K_{t0}T_0}{C_{p0}}\right]s_1 - \frac{l(l+1)}{r^2}\frac{4}{3\kappa_0\rho_0}J_1 - \frac{2}{r}F_r^R - \frac{2}{r}F_r^C - \frac{3}{2}\omega P_{t1} , \tag{13}$$

$$\frac{dP_{t1}}{dr} - \frac{P_{t0}}{\rho_0}\frac{d\rho_1}{dr} + \frac{c\beta g L\rho_0 Q_0}{C_{p0}}\frac{\Gamma_0}{\Gamma_0+1}\frac{ds_1}{dr}$$
$$= -\frac{P_{t0}}{\rho_0^2}\frac{d\rho_0}{dr}\rho_1 + \frac{c\beta g L\rho_0 Q_0\Gamma_0(\nabla - \nabla_{ad}')}{H_p(\Gamma_0+1)^2}\left[\left(\Gamma_0+\frac{5}{2}\right)\frac{\rho_1}{\rho_0} + \frac{\kappa_1}{\kappa_0} + (\Gamma_0+1)\frac{Q_1}{Q_0} - 3\frac{T_1}{T_0}\right.$$
$$\left. - \Gamma_0\frac{C_{p1}}{C_{p0}} + \frac{1}{2}\frac{P_{t1}}{P_{t0}}\right] - \left[\frac{D}{L} - \frac{1}{\rho_0}\frac{d\rho_0}{dr}\right]P_{t1} , \tag{14}$$

$$\frac{4}{3}\mu_{t0}\left(\frac{3}{r} + \frac{1}{\rho_0}\frac{d\rho_0}{dr}\right)v_r - 2\mu_{t0}\frac{l(l+1)}{r}v_h + \left(\frac{4}{3}\mu_{t0}\frac{\omega}{\rho_0}\right)\rho_1 + P_1 - \mathscr{P}_r = 0 . \tag{15}$$

Here the quantities P_{t0}, K_{t0}, μ_{t0} will depend on the value of l as described in Paper I.

This system of equations constitutes a set of nine first order differential equations along with one auxiliary equation. Outside the convection zone where $\mu_{t0} = 0$ and $K_{t0} = 0$ the equations reduce to a system of four first order differential equations. As in Paper I the boundary between the viscous and the inviscid layer is chosen to be a little above the convection zone to take into account the penetration into the convectively stable atmosphere. The complete specification of the problem needs two boundary conditions at each boundary, six connection conditions at upper interface between the viscious and inviscid layers, and seven connection conditions at the lower interface. The asymmetry between the two interfaces is due to equation (3) which distinguishes between the rising and falling convective elements (Shaviv and Chitre 1968). It therefore does not become possible to consider penetration into the underlying radiative layers using this equation even though it takes care of penetration into the overlying convectively stable atmosphere.

We use the same boundary conditions as used in Paper I and adopt the following connection conditions at the upper interface,

$$[v_r] = 0 , \quad [\mathscr{P}_r + P_{t1}] = 0 , \quad [\mathscr{P}_h] = 0 , \quad [F_r^R] = 0 , \quad [F_r^C] = 0 , \quad [J_1] = 0 . \tag{16}$$

At the lower interface we need an additional condition which is assumed to be

$$[\rho_1] = 0 \,. \tag{17}$$

The system of equations along with these boundary and connection conditions constitutes a generalized eigenvalue problem where the eigenvalue ω and the associated eigenfunction are to be determined for a specified value of the horizontal harmonic number l. We have solved the system numerically by a finite difference method (Antia 1979), using 500 mesh points in the difference scheme with the mesh spacing varying between 2×10^5 km and 8×10^5 km.

IV. NUMERICAL RESULTS

The system of equations governing viscous nonadiabatic convective modes is solved to get the growth rate ω for a specified value of l. For each value of l there exists a series of real eigenvalues. We refer to the mode with highest eigenvalue, the fundamental mode, as C1 mode and the successive harmonics by C2, C3, ... We have adopted a value of $\frac{1}{3}$ for the Prandtl number σ_t in most of our calculations. This choice is evidently arbitrary, but, as will be clear from the results, our conclusions are not affected by this choice. Figure 3 displays the growth rate of C1 and C2 modes as a function of l for the model B (*continuous curves*) and model C (*dashed curves*). It can be seen that for the fundamental (C1) mode the growth rate is highest for $l = 1$ while the C2 mode has a maximum growth rate at $l = 2$. We may therefore conclude that the convective modes with very small values of l will dominate, thus supporting Schwarzschild's (1975) assertion. The e-folding time $(1/\omega)$ for the C1 mode is about 30–40 days, while the corresponding value for the C2 mode is of the order of 100–200 days. Further it should be noted that for model B only 12 ($l = 1$–8: C1; $l = 1$–4: C2) and for model C only 19 ($l = 1$–15: C1; $l = 1$–4: C2) modes are found to be unstable. For the model A, only nine ($l = 1$–5: C1; $l = 1$–4: C2) modes are found to be unstable, while the growth rates are higher by about a factor of 20 for $l = 1$; hence we have not displayed the results in the figure. We believe that these abnormally large values are due to the fact that the convection zone extends almost up to the center, where the acceleration due to gravity and consequently the critical growth rate ω_{cr} are very large. These modes are all concentrated near the base of the convection zone. This is in sharp contrast to the solar convection zone where a few thousand modes are found to be unstable and also at small l values the growth rates are very small. This difference is probably due to the extensive convection zone with large viscous damping in the red giants.

For the solar convection zone it is found that the turbulent pressure gives rise to a double peak in the curve of growth rate versus l. In red giants the turbulent pressure is very large; even then we find only one peak in this curve. We think that this is an artifact of very large viscous dissipation in red giants, since both W and L are very large over a substantial portion of the convection zone. This large viscous dissipation may wipe out the second peak completely. To test this conjecture we calculate the growth rates for model B with $\sigma_t = 0.05$, and the results are displayed in Figure 3 (*dotted curves*). In this case the growth rates are, of course, higher than those with $\sigma_t = \frac{1}{3}$, and interestingly we find a second peak in the growth rate for the fundamental mode around $l = 12$, thus confirming our belief. However, in contrast to the solar case, here the first peak at lower l is found to be dominant, and hence as σ_t is increased, the second peak is wiped out, with all the growth rates in that range becoming negative. But it should be noted that even for $\sigma_t = 0.05$ the C1 mode has a maximum growth rate for $l = 1$ and C2 mode at $l = 2$. Thus the position of the main peak is insensitive to the value of σ_t and further for $l = 1$, the growth rate of C1 mode increases by less than 10% when σ_t is decreased from $\frac{1}{3}$ to 0.05. However, at higher l the effect of viscous damping is significant, which clearly is the result of viscous dissipation becoming more effective at smaller length scales.

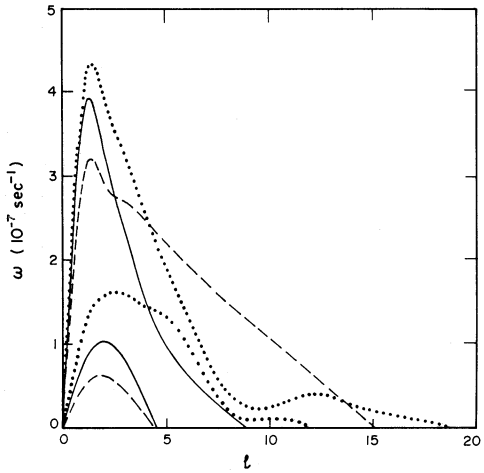

FIG. 3.—The growth rates of the fundamental (C1) mode and the first harmonic (C2) mode are plotted as functions of horizontal harmonic number l. The continuous curves correspond to model B for a choice of the turbulent Prandtl number $\sigma_t = \frac{1}{3}$, and the dotted curves are for the same model with $\sigma_t = 0.05$, while the dashed curves are for model C with $\sigma_t = \frac{1}{3}$.

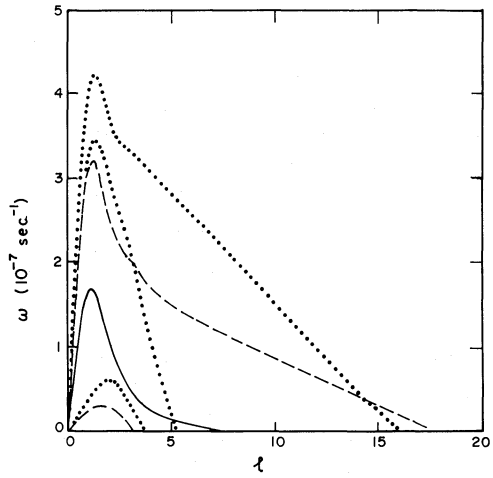

FIG. 4.—The growth rate of convective modes is plotted as a function of l for a choice of $\sigma_t = 1/3$. The continuous curve corresponds to C1 mode for model E, while the dotted curves are for C1, C2, and C3 modes for model D and the dashed curves correspond to the C1 and C2 modes for model F.

The influence of turbulent pressure on the stability of convective modes is studied by considering model D, where turbulent pressure is neglected. The results are displayed in Figure 4 (*dotted curves*); it can be seen that the growth rates have increased considerably, particularly for the C2 mode, which in this case has a maximum at $l = 1$. For this model C3 mode is also found to be unstable for $l = 1$, 2, and 3 with maximum growth rate at $l = 2$. Thus, as in the solar case, here also the turbulent pressure tends to stabilize the convective modes. Also displayed in Figure 4 are the results for the models using the local mixing length theory. For that model the turbulent pressure is found to have a strong stabilizing influence, and the growth rate for $l = 1$ C1 mode is reduced by a factor of 2. This strong influence may be due to abnormally large gradients of turbulent pressure in this model.

V. A PRESCRIPTION TO IDENTIFY THE MIXING LENGTH

In Paper II we have demonstrated the consistency of the mixing length theory for the solar envelope model. It is interesting to examine the same question for the red giants also. This is particularly important since, as noted in the previous section, only about 10–20 of the convective modes are unstable in the envelope of giants and hence it is not clear if a linear superposition of these modes can reproduce the convective flux used in model calculations. As in Paper II, we attempt a least squares fit, but here we use all the unstable modes to get the corresponding weights, and the results for model C are displayed in Figure 5. The continuous curve is the luminosity profile due to the linear superposition of all the modes, while the dashed curve shows the model convective luminosity. It is evident that the two curves agree roughly, thus demonstrating that it is possible to get a reasonable fit to the model flux by using a suitable superposition of convective modes. The luminosity contribution due to some of the individual modes is also displayed by dotted curves in Figure 5. It can be seen that the C1 mode for $l = 1$ accounts for a large fraction of the luminosity in most of the

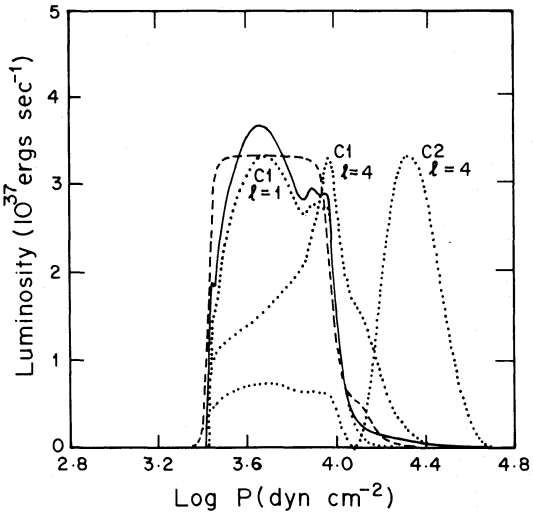

FIG. 5.—The dotted curves show the convective luminosity due to individual C1 modes for $l = 1$ and 4, and C2 mode for $l = 4$, as a function of logarithm of pressure for model C. The continuous curve shows superposed convective luminosity profile, while the dashed curve represents the model convective luminosity.

convection zone, while the C2 modes have peaks in deeper regions of convection zone where only a very small fraction of the flux is transported by convection. Further, the temperature fluctuations obtained by superposition of these modes is found to be about 300–400 K near the top of the convection zone. Similar results were also obtained for model B, but for model A it was found to be rather difficult to get a reasonable fit to the model flux since most of the modes peaked near the base of the convection zone due to the abnormally large value of the critical growth rate ω_{cr} in those regions. This raises an important question, whether it is possible to discard some of the models by requiring consistency and whether the mixing length can be estimated by invoking consistency requirements.

We attempt to identify the mixing length with some scale associated with the individual convective modes. For the solar convection zone, Figure 1 of Paper II shows that the flux profiles due to convective modes with different values of l peak at different depths. Hence it is tempting to identify the mixing length at a particular depth with some length scale of the convective mode which has a peak in flux profile at that depth. We choose the full width at half-maximum for that mode as the natural choice for the length scale. Figure 6 displays the mixing length as a function of logarithm of pressure for the solar envelope model. Also shown are the curves of $2H_p$ and the full width at half-maximum W_h for C1 modes. It can be seen that there is a general agreement between the two curves and further the agreement will improve if we introduce a constant factor of order unity and try to identify the mixing length with a constant multiple α_L of full width at half-maximum. A value of about 0.9 seems to be optimum for α_L.

We shall consider the same problem for the red giant. It is quite clear from Figure 5 that in this case it is difficult to define the full width at half-maximum, and hence we use the equivalent width, defined as

$$W_{eq}(l, n) = \frac{\int 4\pi r^2 F_{l,n}\, dr}{[4\pi r^2 F_{l,n}]_{max}}, \tag{18}$$

where $F_{l,n}$, defined in Paper II, is the convective flux due to the individual linear mode, and the integration extends over the entire convection zone. We further assume the effective depth of this mode to be the point where the contribution to the integral is exactly half the total value. This prescription is, of course, not unique, and we may as well have chosen a different weight function in the integral to get a slightly different value for the effective depth. The results are displayed in Figures 7 and 8 for models B and C, respectively. The points corresponding to different modes are marked in these figures, which also display the plot of mixing length against logarithm of gas pressure. These points fall in two bunches corresponding to the C1 and C2 modes. It should be noted that the numerical uncertainties resulting from the arbitrariness in the definition of equivalent width as well as from the calculated eigenfunctions will lead to uncertainties in both the abscissae and the ordinates of these points. Consequently, it will be more meaningful to consider distance from the curve rather than the difference in ordinates as a measure of departure. It is clear from the figures that the agreement is better for model C, and hence the value of 0.75 for L/H_p seems to be preferred. It should perhaps be stressed that we have employed a nonlocal mixing length prescription to demonstrate the consistency of the model convective luminosity profile with that obtained by the superposition of the linear modes. Clearly, the structure of the convection zone would be significantly affected if we were to adopt a local mixing length formulation, and in particular a choice of 0.75 for the value of the mixing length to scale height ratio need not necessarily apply to models constructed using the local theory. It is not obvious that this value will also be applicable to other classes of stars; in fact, such studies may hopefully show us the way to estimate the mixing length in envelopes of different stars.

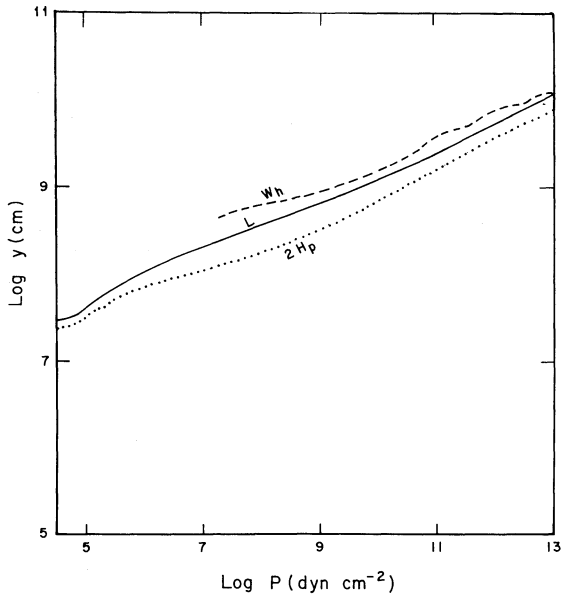

FIG. 6.—The full width at half maximum W_h of the dominant convective mode at a given depth, the mixing length ($L = z + 459$ km) and the curve $y = 2H_p$ are displayed as functions of logarithm of pressure for the solar envelope model.

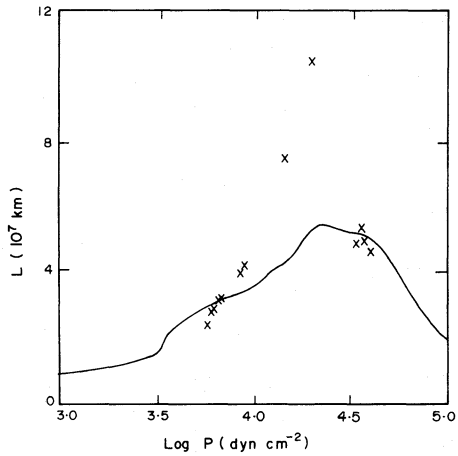

FIG. 7.—The mixing length is plotted against logarithm of the pressure for model B. The equivalent width of the luminosity profile of various convective modes is indicated by crosses.

VI. SUMMARY AND CONCLUSIONS

We have investigated the linear stability of convective modes in the envelopes of red giants to find that modes with smallest values of l (i.e., $l = 1$) have a maximum growth rate. This indicates that in the red giants convective modes with the smallest values of l will dominate the brightness fluctuations and only a small number of such large "granules" occupy the surface of the star at any given time. The granules can cause significant variations in the integrated stellar light on a time scale of the order of the e-folding time for these modes which comes out to be about 40 days for the red giant model considered here. Clearly the e-folding time for the maximally growing convective mode is within the observed characteristic time of irregular variation of red giants. It is also demonstrated that even with only 10–20 unstable modes it is possible to construct a linear superposition of these modes which can reproduce the model convective flux reasonably well. Further, the amplitude of convective modes determined through the fitting of the model flux yields temperature fluctuations of approximately 300–400 K at the stellar surface. This can account for the observed luminosity fluctuation of a factor of 2 in the visible light which is the typical observed amplitude for irregular variations. Thus our work strongly supports Schwarzschild's (1975) conjecture that the fluctuations caused by extremely large convective elements in the photosphere of red giants can explain the observed phenomenon of irregular variation, a characteristic of all late type stars having extensive convection zones. Naturally, in many cases the irregular variations could be superposed on regular variations due to pulsation.

It is worthwhile to add a cautions note about our modal analysis performed in the linear regime, as such an approach is supposed to represent a highly turbulent nonlinear phenomenon with the help of linearized equations. We have investigated the stability of the linear modes with the assumption that the coupling between modes is incorporated through the turbulent transport coefficients. The nonlinear effects are thus very crudely taken into account in the analysis, which is then checked for consistency by superposition of the linear convective modes to enquire whether the model convective

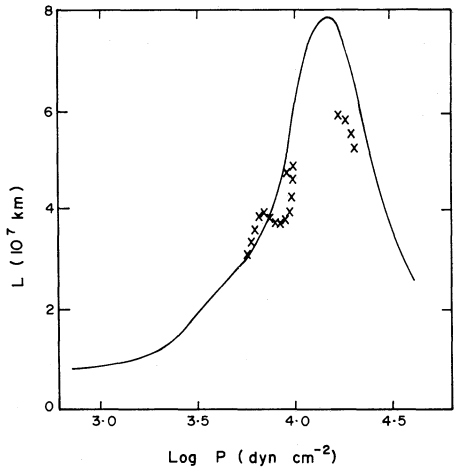

FIG. 8.—The mixing length is plotted against logarithm of the pressure for model C. The equivalent width of the luminosity profile of various convective modes is indicated by crosses.

luminosity profile can be reasonably reproduced at every level in the envelope. Naturally, we cannot demonstrate that the nonlinear effects included through the eddy coefficients and the explicit calculation of the mode coupling are equivalent.

In conclusion, we should emphasize that the nonlocal version of the mixing-length theory is very effective in the computation of stellar models when the turbulent pressure is included in the governing equations of stellar structure. It also seems plausible to identify the mixing length with the equivalent width of the luminosity profile of various convective modes. On the basis of this identification we conclude that for the red giant model considered here the ratio of mixing length to pressure scale height should be around 0.75. It will be interesting to find this ratio for stars belonging to other luminosity classes.

It is a pleasure to thank Professor Martin Schwarzschild for a valuable discussion.

REFERENCES

Antia, H. M. 1979, *J. Comp. Phys.*, **30**, 283.
Antia, H. M., Chitre, S. M., and Narasimha, D. 1983, *M.N.R.A.S.*, **204**, 865 (Paper I).
Baker, N., and Gough, D. O. 1979, *Ap. J.*, **234**, 232.
Fox, M. W., and Wood, P. R. 1982, *Ap. J.*, **259**, 198.
Hart, M. H. 1973, *Ap. J.*, **184**, 587.
Henyey, L. G., Vardya, M. S., and Bodenheimer, P. L. 1965, *Ap. J.*, **142**, 841.
Keeley, D. A. 1970, *Ap. J.*, **161**, 657.
Krishna Swamy, K. S. 1966, *Ap. J.*, **145**, 174.
Narasimha, D., and Antia, H. M. 1982, *Ap. J.*, **262**, 358 (Paper II).
Payne-Gaposchkin, C. 1954, *Variable Stars and Galactic Structure* (London: Athlone Press).
Ralston, A. 1965, *First Course in Numerical Analysis* (New York: McGraw Hill).
Schwarzschild, M. 1975, *Ap. J.*, **195**, 137.
Shaviv, G., and Chitre, S. M. 1968, *M.N.R.A.S.*, **140**, 61.
Stothers, R. C. 1972, *Astr. Ap.*, **18**, 325.
Strohmeier, W. 1972, *Variable Stars* (New York: Pergamon).
Tuchman, Y., Sack, N., and Barkat, Z. 1979, *Ap. J.*, **234**, 217.
Willson, L. A. 1982, in *Pulsation in Classical and Cataclysmic Variable Stars*, ed. J. P. Cox and C. J. Hansen, p. 269.
Wood, P. R. 1974, *Ap. J.*, **190**, 609.
———. 1975, in *IAU Colloquium 29, Multiple Periodic Variable Stars*, ed. W. S. Fitch (Dordrecht: Reidel), p. 69.
———. 1982, in *Pulsation in Classical and Cataclysmic Variable Stars*, ed. J. P. Cox and C. J. Hansen, p. 284.

H. M. ANTIA, S. M. CHITRE, and D. NARASIMHA: Theoretical Astrophysics Group, Tata Institute of Fundamental Research, Homi Bhabha Road, Bombay 400 005, India